ROYAL SOCIETY
OF CHEMISTRY

PAPER

Check for updates

Insights into the interface reaction between electrolyte and Li$_2$MnO$_3$ from *ab initio* molecular dynamics simulations†

Xiaotong Yan,[a] Chunwei Zhu,[a] Weijie Huang[a] and Yu-Jun Zhao ⓘD *[ab]

The complex interface reaction plays a critical role in the Li$_2$MnO$_3$ cathode material with high energy density. Here, the interface reactions between the liquid electrolyte molecules and the typical surfaces of Li$_2$MnO$_3$ are systematically investigated by *ab initio* molecular dynamics (AIMD) simulation and first-principles calculation. We demonstrate that the decomposition of electrolyte molecules on the different surfaces of Li$_2$MnO$_3$ exhibits a high degree of similarity. The carbonyl carbon (C_C) and ether oxygen (O_E) of the electrolyte molecule that bind to the O and Mn of the Li$_2$MnO$_3$ surface, respectively, are the prerequisites for the decomposition of the electrolyte molecules. The redox reaction between the electrolyte molecule and the surface of Li$_2$MnO$_3$ considerably weakens the strength of the C_C-O_E bond. In particular, the surface of (001) is an inert surface, which does not react with electrolyte molecules through our AIMD simulations. This is due to the large electron occupation energy gap between the electrolyte molecule and the (001) surface. This study provides a theoretical insight into the interface reaction between lithium-rich cathode materials and liquid electrolytes.

1 Introduction

Lithium-rich cathode materials (LRCMs), with ultra-high energy densities exceeding 300 mA h g^{-1}, are strong candidates for solving the range problem of electric vehicles and large-scale energy storage applications.[1–3] The cathode material Li$_2$MnO$_3$ attracts much attention due to its high voltage (up to 4.5 V), high specific capacity (theoretical capacity of up to 458 mA h g^{-1}), cost effectiveness and environmental friendliness.[4,5] However, the complex surface reactions can negatively affect stability, safety, and energy density during the cycle.[4,6–8]

In general, a multitude of side reactions occur at the interface between cathode materials and liquid electrolytes during the cycle. These reactions not only consume limited amounts of cathode material and electrolyte but also lead to the formation of inert cathode-electrolyte interphase (CEI) films and gases.[1,6]

Researchers have performed a significant amount of work to mitigate this issue. Yan *et al.*[9] investigated the mechanism of structural evolution of Li$_2$MnO$_3$, and their results indicate that the structural evolution of Li$_2$MnO$_3$ proceeds from the surface to the interior. Li *et al.*[10] reported LRCMs coated with Al$_2$O$_3$ using a combination of atomic layer deposition (ALD) and bulk

phase modulation techniques. These modified cathode materials have demonstrated improved cycling stability and safety. Wei *et al.*[11] utilized the solid acid Zr(HPO$_4$)·H$_2$O to modify the surface of manganese-based LRCMs, effectively inhibiting the release of oxygen and the occurrence of surface side reactions. Additionally, Chen *et al.*[12] investigated the deposition of S on the surface of LRCMs based on the properties of polyanionic polymers. Their research demonstrated that the surface deposition of S can lead to the formation of a $(SO_n)^{m-}$ polyanion layer, which interacts with the surrounding O ions, thereby enhancing the cycling stability of LRCMs. Si *et al.*[13] utilized the piezoelectric material LiTaO$_3$ to coat LRCMs, which not only enhances the structural stability, but also improves the diffusion properties of Li$^+$ at the interface through its piezoelectric properties. Zhu *et al.*[14] employed MoO$_3$ as a surface reagent. This reagent reacts with LiO precipitates near the surface of LRCMs, thereby increasing the concentration of transition metals. The findings indicate that the valence of transition metal (TM) ions is reduced, and the oxidation and evolution of O ions are effectively mitigated.

To sum up, there are numerous reports focusing on improving the performance of LRCMs.[15–23] However, the interfacial reaction mechanisms between Li-rich cathode materials and electrolytes have been rarely reported. This can be attributed to the complexity and dynamics of interface reactions, which pose significant challenges even when *in situ* characterization techniques are employed.[24–26]

The first-principles calculation and *ab initio* molecular dynamics (AIMD) have proven effective in addressing this

[a]Department of Physics, South China University of Technology, Guangzhou 510640, PR China. E-mail: zhaoyj@scut.edu.cn

[b]Key Laboratory of Advanced Energy Storage Materials of Guangdong Province, South China University of Technology, Guangzhou 510641, China

This journal is © The Royal Society of Chemistry 2024

J. Mater. Chem. A, 2024, **12**, 24401–24408 | **24401**

issue.[27–31] Through molecular dynamics simulations, Zhang *et al.*[32] demonstrated that the defective CEI material LiF reacts with $LiPF_6$ at the interface. Qin *et al.*[33] conducted a theoretical study of the decomposition of ethylene carbonate (EC) molecules on the (110) surface of both $LiCoO_2$ and $LiNi_{1/3}Co_{1/3}Mn_{1/3}O_2$. Their study indicates that the initial stage of this reaction involves a ring-opening reaction of C_C–O_E cleavage. Subsequently, the H from the electrolyte molecule adsorbs onto the cathode surface. In addition, theoretical research has identified an oxygen release phenomenon occurring with pure $Li_{1.2}Ni_{0.6}Mn_{0.2}O_2$ cathode materials across various Li ion concentrations. It has been shown that sulfur doping can significantly suppress oxygen release during the charging process.[34] However, the interface reactions between Li_2MnO_3 and electrolyte have not been well studied, in either experimental or theoretical contexts.

In this study, we employ AIMD simulations to effectively model the interface reactions between liquid electrolytes and the typical surfaces of Li_2MnO_3, which are characterized in our previous research.[35] We then carefully examine the interface stability, reaction barrier, electronic structure and reaction mechanism of electrolytes on these surfaces of Li_2MnO_3. Our finding reveals that the C_C and O_E atoms of electrolyte molecules engage in charge transfer (binding) with the O and Mn ions on the Li_2MnO_3 surfaces during the adsorption stage. Consequently, the bond strength of C_C–O_E is thus greatly weakened. Finally, we summarize the similarities of reactions of electrolyte molecules on different surfaces of Li_2MnO_3, and offer a theoretical explanation to elucidate the interfacial reaction between electrolyte molecules and surfaces of the Li_2MnO_3 cathode material.

2 Computational details

2.1 Computational methods

The AIMD simulations and first-principles calculation are performed using the projector augmented wave (PAW) scheme,[36] as implemented in the Vienna *Ab initio* Simulation Package (VASP).[37,38] The exchange-correlation energies are approximated with the generalized gradient approximation (GGA) of Perdew, Burke, and Ernzerhof (PBE).[39] For AIMD simulations, the NVT ensemble is employed at an equilibrium temperature of 400 K for a total time of 10 ps with a time interval of 1 fs.[31,32,34] The cutoff energy for the plane wave expansion is set to 400 eV, and the convergence criterion for the electronic self-consistent iteration is 1×10^{-4} eV. According to ref. 40–44 and our test results, the van der Waals (vdW) interaction is not considered in AIMD simulations, as it does not affect our main conclusions (see Sections S7 and S8 of the ESI†). For subsequent property studies based on first-principles calculations, the vdW interaction (DFT-D3 method of Becke–Johnson[45]) and the cutoff energy option of 650 eV are used to improve the accuracy of calculations. The ionic positions are relaxed until the forces on each ion converge to less than 0.01 eV $Å^{-1}$. The climbing image nudged elastic band (CINEB) method is used to obtain energy barriers for electrolyte molecule decomposition.[46] In addition, to account for the on-site Coulomb interactions for the localized

3d electrons of transition metals, an additional Hubbard parameter correction is applied according to ref. 47 and 48 Within the GGA + U scheme, a single effective parameter $U_{eff} = U - J$ is used, and an U_{eff} value of 4.5 eV for Mn is determined by the deintercalation voltage and band gap tests, which are in good agreement with the experiment.[4,49] The gamma point of the Brillouin zone is sampled without consideration of the symmetry of systems. Spin polarization is taken into all the calculations.

2.2 Computational model and process

The primary focus of this work is on constructing an interface model and subsequently calculating and analyzing its properties. First, our AIMD calculations are based on an interface model that includes a liquid electrolyte and the typical surface of Li_2MnO_3. Here, the liquid electrolyte is composed of ethylene carbonate (EC), dimethyl carbonate (DMC), and lithium hexafluorophosphate ($LiPF_6$), with a volume ratio of EC to DMC of 1 : 1 and a $LiPF_6$ concentration of 1 mol L^{-1} in EC/DMC.[32] To ensure the reliability of AIMD calculations, a stable electrolyte cluster is meticulously investigated and subsequently used. The typical surfaces for the interface model are selected from our previous work,[35] including the (010), (10$\bar{1}$), (131), and (001) planes. A slab model, consisting of at least five atomic layers, is employed to simulate the surface structure, with one-third of the slab's thickness fixed to the bulk structure. The stability analysis of the electrolyte cluster, the selection of typical surfaces, and the process of creating the interface model are detailed in Section S1.† Ultimately, employing the computational method outlined in Section 2.1, we calculate and analyze the relevant properties of the interface. A schematic diagram of the research process is depicted in Fig. 1.

3 Results and discussion

To clarify the interface reaction between the electrolyte molecules and the various surfaces of Li_2MnO_3, the AIMD simulations for each distinct interface are analyzed and discussed in this section. First, we described the decomposition process of electrolyte molecules during the AIMD simulations. Subsequently, we extracted the initial and final states of these decomposition structures and calculated the energy barriers for their decomposition (see Section S3.5† for detailed calculations of the energy barriers). Finally, we studied the properties exhibited during the decomposition of electrolyte molecules and explained these properties by analyzing the changes in electronic structure throughout the decomposition process. In the following figures, ISO stands for an isolated molecule or surface. The acronyms of IS, TS, and FS represent the initial, transitional, and final states, respectively, of different interfaces during the process of electrolyte molecule decomposition. In this study, the (001) surface is identified as inert. It exhibits no reaction with electrolyte molecules, regardless of the AIMD simulations conducted (further details are available in Sections S4 and S8†). A comprehensive explanation is provided in Section 3.4.
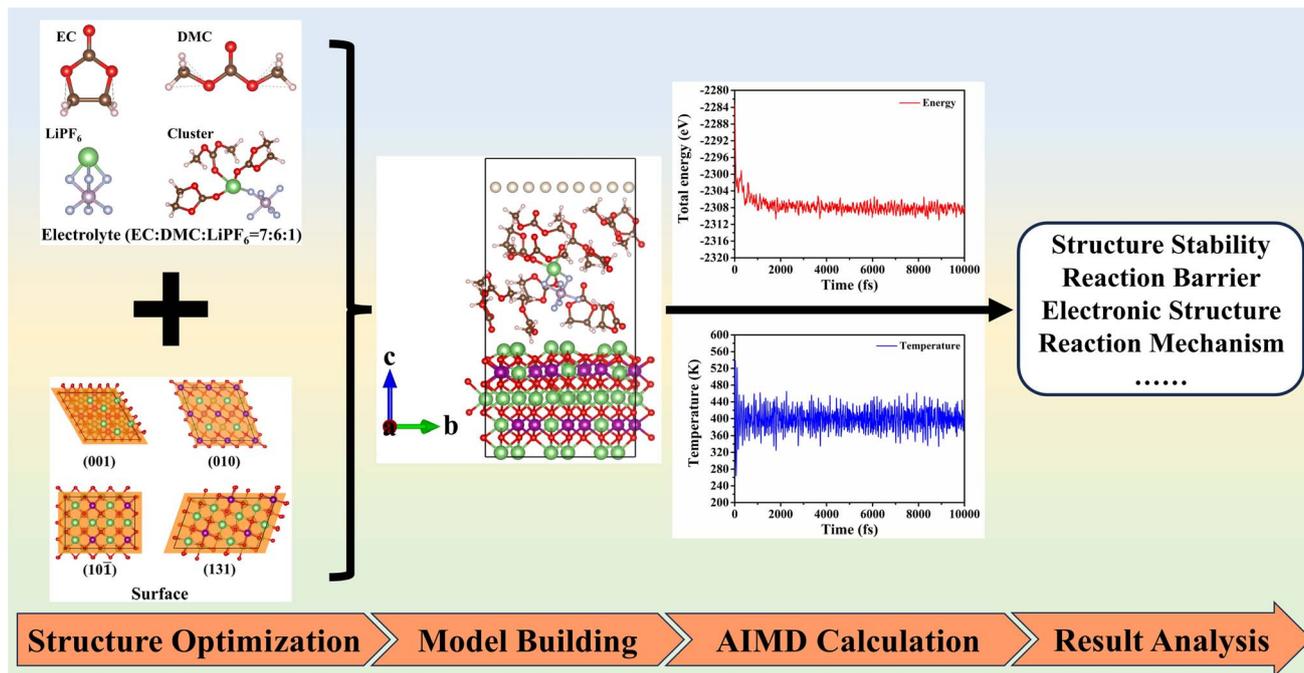
24402 | *J. Mater. Chem. A*, 2024, **12**, 24401–24408

This journal is © The Royal Society of Chemistry 2024

Fig. 1   The schematic diagram of the research process for the interface reaction of liquid electrolyte and the Li_2MnO_3 surface.

3.1   The interface reaction of the (010) surface

The results of the interface reaction of the electrolyte molecule on the (010) surface show that the EC molecule is decomposed. The relevant data on the decomposition of the EC molecule are shown in Fig. 2. By examining Fig. 2(a) and (b), we observe the following sequence of events regarding the decomposition of the EC molecule on the (010) surface:

(i) The O_C of the EC molecule becomes adsorbed onto Mn1 of the (010) surface. (ii) Overtime, the distances between the C_C and O_E of the EC molecule and the O and Mn2 of the (010) surface decrease. (iii) At the time of 2.96 ps, the EC molecule is stably adsorbed on the (010) surface, marking the commencement of its decomposition reaction. (iv) Subsequently, the distance between C_C and O_E of the EC molecule increases progressively over time. (v) Commencing at 3.08 ps, the bond lengths of C_C–O and O_E–Mn2 remain constant, whereas the bond of C_C–O_E is broken. This observation suggests that the EC molecule undergoes a ring-opening reaction on the (010) surface.

To ascertain the difficulty of the ring-opening reaction for the EC molecule on the (010) surface, we calculated the energy barrier associated with the decomposition process, as depicted in Fig. 2(c). The calculated energy barrier for the decomposition of the EC molecule is found to be minimal, at only 4 meV (see Section S3.5†). This low value suggests that the decomposition of the EC molecules on the (010) surface is likely to occur spontaneously.

To address this issue, we have analyzed the changes in the electronic structure, specifically the partial density of states (PDOS) of the EC molecule as it decomposes on the (010) surface. As illustrated in Fig. 2(d), there are minimal changes in the electronic occupancy states for the Mn, O, O_E, and C_C (*c.f.*

Fig. 2(c)) during the transition from the initial state (IS) to the transitional state (TS). This proves that no remarkable charge transfer occurs during this process. At the same time, the Bader charges for the Mn, O, O_E, and C_C have also been calculated across different states. Fig. 2(e) shows that the charges of C_C and O_E change significantly before and after adsorption. In contrast, the charge changes for Mn and O ions at the (010) surface are not obvious, which may be attributed to the redistribution of surface charge. However, the Bader charges for Mn, O, O_E, and C_C remain almost unchanged during the transition from the IS to the TS. This constancy, as depicted in Fig. 2(e), further supports the notion that no charge transfer occurs during the transition. The above analysis indicates that any charge transfer between the relevant ions during the adsorption process should influence the energy barrier. The charge density difference $\Delta\rho$ (see Fig. 2(f)) of EC and the (010) surface after adsorption is thus calculated according to formula (1).

$$\Delta\rho = \rho_{ads} - \rho_{surf} - \rho_{mol}, \qquad (1)$$

where ρ_{ads}, ρ_{surf}, and ρ_{mol} correspond to the charge densities of the adsorption structure, the isolated surface, and the isolated molecule, respectively. From Fig. 2(e) and (f), it can be observed that the C_C of the EC molecule has lost a significant number of electrons, while the O atom on the (010) surface gains electrons through its interaction with the C_C of the EC molecule. Additionally, the O_E of the EC molecule receives electrons from the Mn ion of the (010) surface, forming a bond with it. In particular, electrons near the C_C in the C_C–O_E bond are particularly affected, indicating a high degree of electron loss. This suggests that the redox reaction during the decomposition of the EC molecule is predominantly occurring during the adsorption stage. The bond
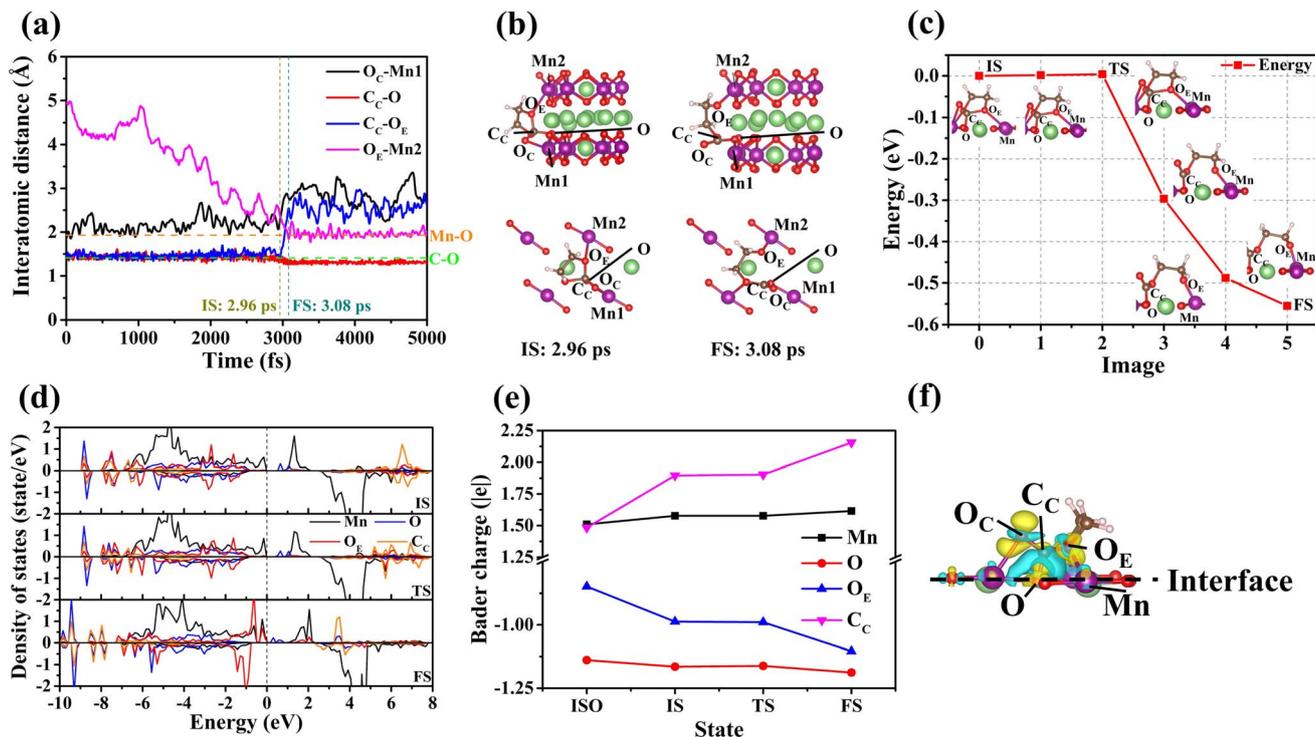
Fig. 2 (a) The changes in atomic distance upon decomposition of EC on the (010) surface. (b) and (c) The schematic diagram and energy barrier of EC decomposition on the (010) surface. (d) and (e) The partial density of states (PDOS) and Bader charges of Mn, O, O_E, and C_C in different states. (f) The charge density difference between the EC and the (010) surface after adsorption (the iso-surface charge density is assumed to be 5×10^{-3} e bohr^{-3}).

strength of the C_C–O_E bond is greatly reduced, resulting in the energy barrier for the EC ring-opening being close to zero. In addition, it can be observed from Fig. 2(d) and (e) that some charge transfer also occurs during the transition from the transitional state (TS) to the final state (FS). This could be attributed to the charge transfer facilitated by the decrease in the distance for C_C–O and O_E–Mn, which allows for the formation of more stable bonds.

3.2 The interface reaction of the (10$\bar{1}$) surface

The EC molecule decomposes at the interface between the liquid electrolyte and the (10$\bar{1}$) surface. The corresponding results of EC decomposition are shown in Fig. 3. Fig. 3(a) and (b) illustrate that the decomposition of the EC molecule occurs through the following steps:

(i) The Li1 of the surface adsorbs the O_C of the EC molecule. (ii) The distances between C_C–O and O_E1–Mn1 decrease over time. (iii) The EC molecule becomes stably adsorbed on the surface and initiates dissociation at 1.00 ps. (iv) As time continues to increase, the distance between C_C and O_E1 of the EC molecule gradually increases. (v) From 1.30 ps onwards, the bond lengths of the C_C–O and O_E1–Mn1 bonds remain unchanged. However, the bond between C_C and O_E1 breaks, and ring-opening occurs within the EC molecule.

The energy barrier for the decomposition process of the EC molecule on the (10$\bar{1}$) surface has been calculated to ascertain the difficulty of the ring-opening reaction, as depicted in Fig. 3(c). According to Fig. 3(c), the energy barrier during the

decomposition of the EC molecule is nearly zero, with a value of only 0.2 meV (see Section S3.5†). This suggests that the decomposition of EC molecules on the (10$\bar{1}$) surface is spontaneous. To further investigate this finding, the electronic structure of the EC molecule during decomposition on the (10$\bar{1}$) surface has been calculated (c.f. Fig. 3(d)). The electronic occupation states of Mn, O, O_E, and C_C (as seen in Fig. 3(c)) exhibit minimal changes from the IS to the TS, indicating that this process does not clearly involve a charge transfer. Additionally, the Bader charges of Mn, O, O_E, and C_C have been calculated across different states (c.f. Fig. 3(e)). Although the charges of C_C and O_E of the EC change significantly during adsorption, the Bader charges for Mn, O, O_E, and C_C remain constant throughout the transition from the IS to the TS. This consistency further supports the absence of charge transfer from the IS to the TS. Consequently, the energy barrier may be influenced by charge transfer between the relevant ions during the adsorption process. Fig. 3(f) illustrates the charge density difference before and after the adsorption of the EC molecule on the (10$\bar{1}$) surface. From Fig. 3(e) and (f), it is observed that the C_C in the EC molecule has lost a significant number of electrons. These electrons are transferred to the O atom of the (10$\bar{1}$) surface as a result of the binding interaction. Additionally, due to the binding, the O_E of the EC molecule receives electrons from the Mn of the (10$\bar{1}$) surface. In particular, there is a substantial loss of electrons surrounding C_C in the C_C–O_E bond. This indicates that the bond strength of the C_C–O_E bond is greatly reduced, so that the energy barrier is nearly zero.

24404 | *J. Mater. Chem. A*, 2024, **12**, 24401–24408

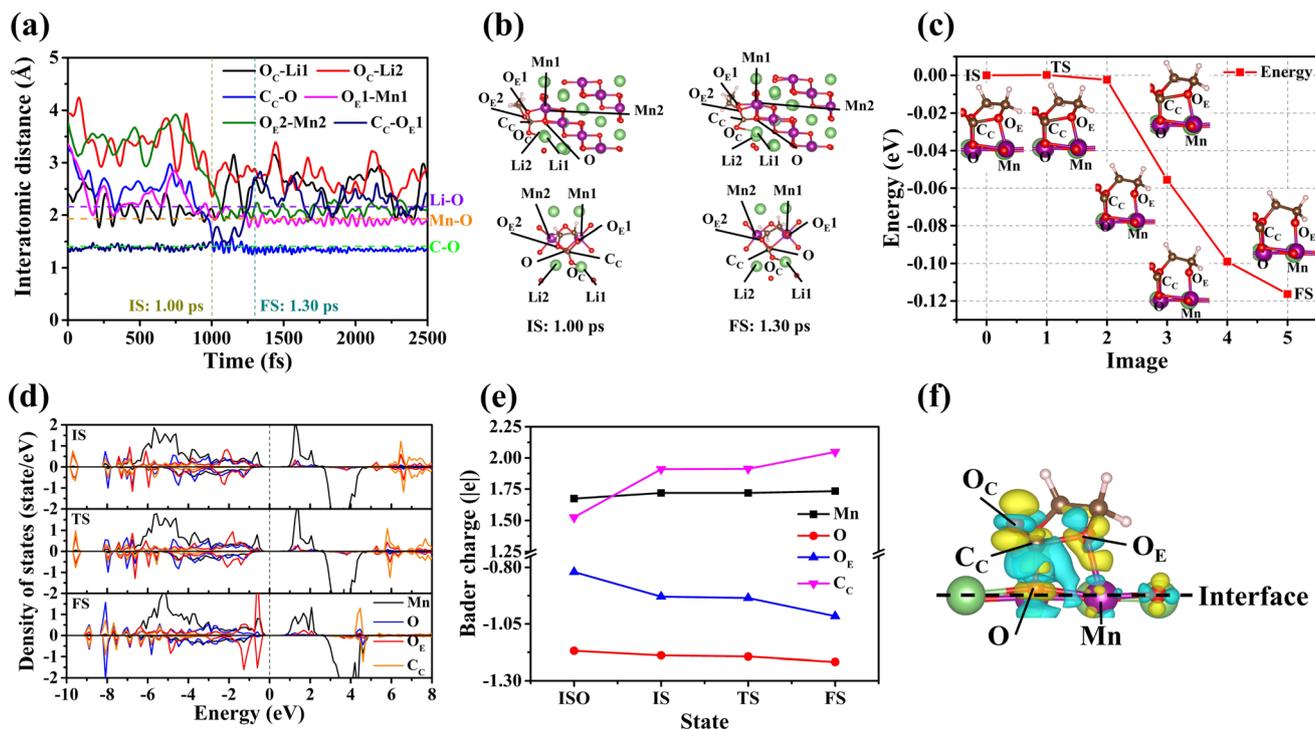This journal is © The Royal Society of Chemistry 2024

Fig. 3 (a) The changes in atomic distance upon decomposition of EC on the $(10\bar{1})$ surface. (b) and (c) The schematic diagram and energy barrier of EC decomposition on the $(10\bar{1})$ surface. (d) and (e) The PDOS and Bader charges of Mn, O, O_E, and C_C in different states. (f) The charge density difference between EC and the $(10\bar{1})$ surface after adsorption (the iso-surface charge density is assumed to be 5×10^{-3} e bohr^{-3}).

3.3 The interface reaction of the (131) surface

Interface reactions take place on the surface of (131). According to the AIMD simulation, the EC and DMC molecules decompose on this surface (DMC decomposition, see Section S5†). Fig. 4 shows the corresponding results of the EC molecule decomposition. As observed in Fig. 4(a) and (b), the decomposition of the EC molecule follows a similar decomposition process to that described previously:

(i) The O_C of the EC molecule is adsorbed onto the Mn1 of the (131) surface. (ii) The distances of C_C–O and O_E–Mn2 decrease over time. (iii) At the time point of 0.67 ps, the stably adsorbed EC molecule initiates the ring-opening reaction on the (131) surface. (iv) The distance between C_C and O_E continues to increase with time. (v) At 1.21 ps, the C_C–O_E bond is broken, while the bond lengths of C_C–O and O_E–Mn2 remain stable.

Similar to the previous results, the energy barrier of the ring-opening reaction of the EC molecule on the (131) surface has been calculated (see Fig. 4(c)). According to Fig. 4(c), there is nearly no energy barrier observed during the decomposition of the EC molecule, with a value of only 7 meV (see Section S3.5†). This minimal energy barrier suggests that the EC molecules decompose spontaneously on the (131) surface. To understand this phenomenon, the electronic structure and Bader charge of the EC molecule on the (131) surface have been calculated for various states (*c.f.* Fig. 4(d) and (e)). From Fig. 4(d) and (e), the electronic occupancies and Bader charges of Mn, O, O_E, and C_C (see Fig. 4(c)) are stable during the transition from the IS to the TS, indicating that no charge transfer occurs during the

transition. However, significant changes in the charges of C_C and O_E of the EC are observed before and after adsorption on the (131) surface. According to the above analysis, the charge transfer between the relevant ions may affect the energy barrier in the adsorption process. The charge density difference of the adsorption of EC molecules on the (131) surface is shown in Fig. 4(f). When Fig. 4(e) and (f) are considered together, a similar conclusion can be drawn. The C_C of the EC molecule and the O of the (131) surface display distinct electronic behaviors, with the C_C releasing electrons and the O atom accepting them, due to their mutual binding. The O_E of the EC molecule also accepts electrons from the Mn of the (131) surface, forming a bond. Consequently, the electrons surrounding the C_C have significantly decreased in the C_C–O_E bond. The bond strength of the C_C–O_E bond is greatly reduced, so that the energy barrier for the EC ring-opening is nearly zero.

3.4 Discussion

Analysis of the above results reveals that the decomposition of the electrolyte molecules (EC/DMC) on the (010), $(10\bar{1})$, and (131) surfaces of Li_2MnO_3 shows an extremely high degree of similarity. This suggests that the decomposition of EC/DMC on the Li_2MnO_3 surfaces can be attributed to a combination of a special adsorption site and a stable electronic structure (redox reaction). The influence of the special adsorption site is illustrated in Fig. 5.

According to the above analysis and as depicted in Fig. 5, the decomposition of the electrolyte molecule (EC/DMC) on the surfaces of Li_2MnO_3 can generally be summarized as follows:

This journal is © The Royal Society of Chemistry 2024

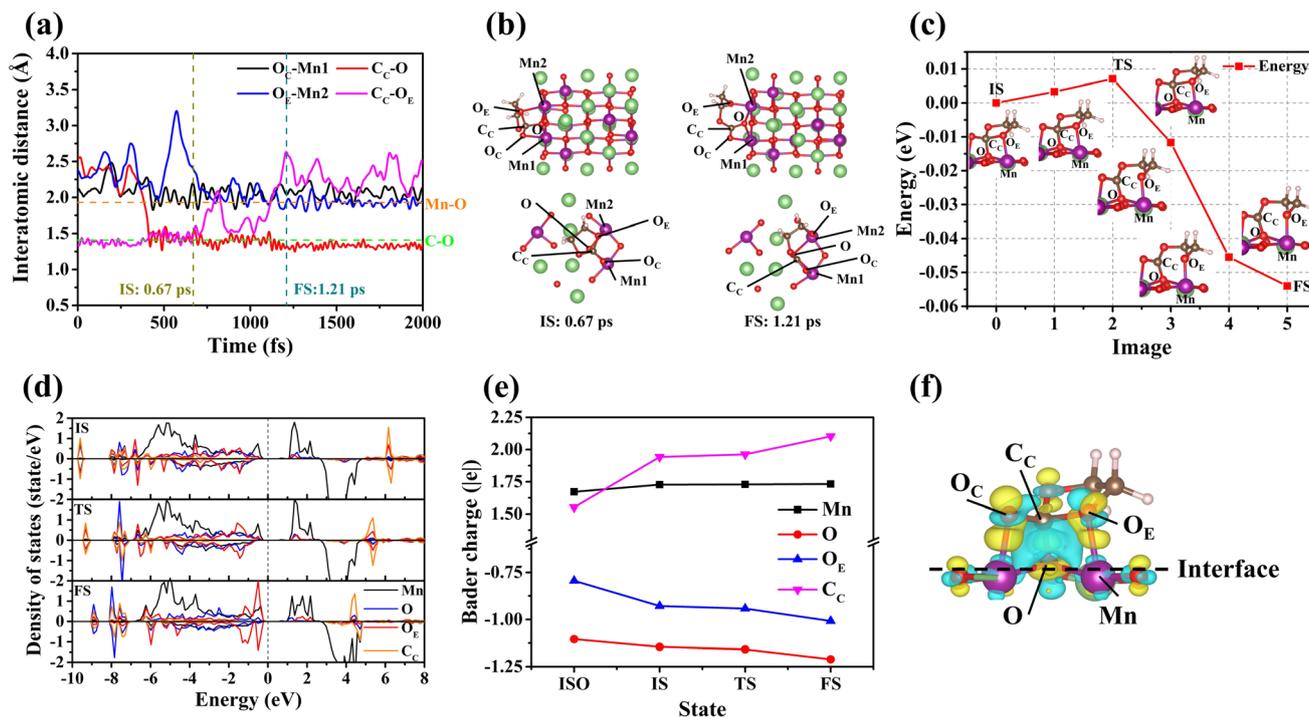*J. Mater. Chem. A*, 2024, **12**, 24401–24408 | **24405**

Fig. 4 (a) The changes in atomic distance upon decomposition of EC on the (131) surface. (b) and (c) The schematic diagram and energy barrier of EC decomposition on the (131) surface. (d) and (e) The PDOS and Bader charges of Mn, O, O_E, and C_C in different states. (f) The charge density difference between EC and the (131) surface after adsorption (the iso-surface charge density is assumed to be 7×10^{-3} e bohr^{-3}).

(I) Localized adsorption: the O_C of the electrolyte molecule adsorbs on to Li/Mn on the surface, which plays a role in positioning. Following this, the C_C and O_E of the electrolyte molecule are adsorbed onto the Li_2MnO_3 surface in the vicinity of this site.

(II) Specific adsorption leading to a decomposition reaction: this study shows that only the effective adsorption and binding of C_C–O and O_E–Mn can trigger the decomposition reaction of the electrolyte molecules. However, the adsorption and binding of C_C–O and O_E–Li do not lead to the decomposition reaction of

Fig. 5 Schematic diagram of decomposition of electrolyte molecules (EC/DMC) on the surfaces of Li_2MnO_3. Only atoms involved in the decomposition of electrolyte molecules are shown.

electrolyte molecules (*c.f.* Sections S6 and S8†). This is mainly due to the strong redox reaction between electrolyte molecules and the Li_2MnO_3 surfaces (the detailed analysis shows the stable electronic structure). As a result, the stable chemical bonds C_C–O and O_E–Mn are formed and the strength of the C_C–O_E bond is greatly weakened. Therefore, the interaction between the electrolyte molecules and the Li_2MnO_3 surfaces is strengthened, while the internal strength of the electrolyte molecules is weakened.

(III) Distortion decomposition: in this study, the different bond lengths and angles between the atoms (ions) of electrolyte molecules and Li_2MnO_3 surfaces induce distortion. This distortion, in turn, leads to the decomposition of the electrolyte molecules, which fulfills the conditions established in step II.

In general, achieving a stable electronic structure is the starting point of a redox reaction. The above analysis shows that a large part of the charge transfer takes place mainly in the adsorption stage. The changes in the occupancy state of electrons before and after the adsorption of electrolyte molecules on Li_2MnO_3 surfaces are illustrated in Fig. 6, which takes into account the above PDOS, Bader charge, and charge density difference data.

Fig. 6 shows that Mn–O and C_C-O_E are bound to the isolated surface and molecule, respectively (old bonds). However, this state is destroyed when the electrolyte molecules are adsorbed at specific sites on the Li_2MnO_3 surface. After adsorption, effective bonds (new bonds) are formed for the C_C–O and O_E–Mn of the electrolyte molecule and the Li_2MnO_3 surface. This is mainly due to the close occupation of the energy levels of the electrons between the binding atoms (ions), along with
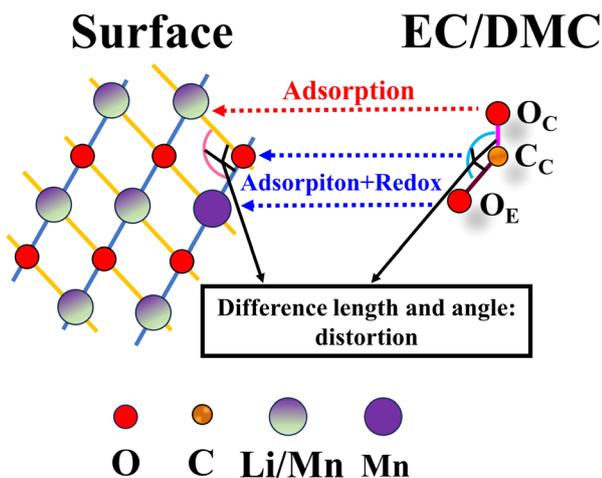
24406 | *J. Mater. Chem. A*, 2024, **12**, 24401–24408
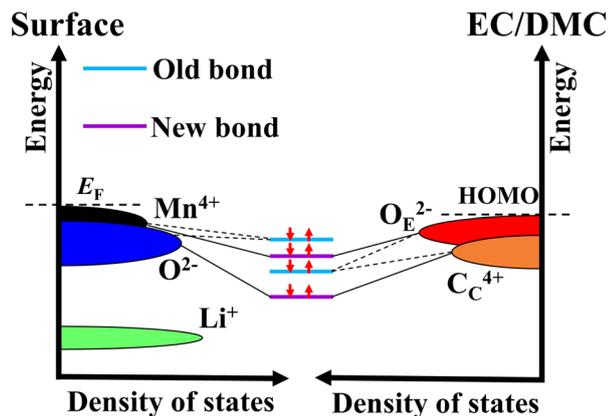
This journal is © The Royal Society of Chemistry 2024

Fig. 6 Schematic diagram of the electronic structure change of electrolyte molecules (EC/DMC) and surfaces of Li_2MnO_3.

a subsequent effective reduction in the electronic energy levels after binding.

In addition, the (001) surface is considered inert in our research, as it does not react with the electrolyte molecules. This behavior can be well explained by referring to Fig. 6. The (001) surface is a stable surface that satisfies the stoichiometric ratio, with the outermost layer composed of Li ions (as detailed in Section S1.2 and ref. 35). However, Fig. 6 indicates that the electron occupation energy level of the Li ion is quite low (the large energy level gap with the electrolyte molecule). This makes it difficult to effectively bond or react (charge transfer) with the electrolyte molecules, which aligns with the findings of relevant experimental studies.[50] Meanwhile, the (001) surface has the highest energy level of occupied electrons compared to other surfaces and electrolyte molecules. As a result, the (001) surface remains inert even under conditions of charging (*c.f.* Section S4†). Similarly, the large energy level gap between the Li ion and the electrolyte molecule also accounts for why the adsorption and binding of C_C–O and O_E–Li does not cause a decomposition reaction of the electrolyte molecules (see Section S6†). This indicates that the stable electronic structure leads to the specificity of the adsorption site.

It should be noted that only the decomposition of the DMC electrolyte molecule at the (131) surface has been observed, albeit due to the limited computational resources. However, the decomposition processes are very similar to the ring-opening process of EC molecules (see Section S5†). Therefore, we postulate that the findings from our discussion on the decomposition of electrolyte molecules on the Li_2MnO_3 surface are also applicable to the DMC molecule, although the primary basis for these conclusions is drawn from the ring-opening reaction of the EC molecule.

4 Conclusion

In summary, we have systematically investigated the interface reaction, reaction barrier, electronic structure, and reaction mechanism between the liquid electrolyte molecules and the typical surfaces of Li_2MnO_3 by the AIMD simulation and first-principles calculation. It is shown that the electrolyte

molecules EC (or DMC) have decomposition reactions on the surfaces of (010), (10$\bar{1}$), and (131), with the exception of the (001) surface, which remains inert. The energy barrier for the decomposition of the electrolyte molecule is nearly zero. This phenomenon is a critical redox reaction caused by the special adsorption of electrolyte molecules on the Li_2MnO_3 surfaces. On one hand, it weakens the internal bond strength (C_C–O_E) of the electrolyte molecule. On the other hand, it strengthens the interaction between the electrolyte molecule and the Li_2MnO_3 surface (C_C–O and O_E–Mn). Additionally, the different bond lengths and angles between the atoms (ions) of the electrolyte molecules and the Li_2MnO_3 surface influence the decomposition of the electrolyte molecules. The inertia of the (001) surface is due to the low electron occupation energy level of Li ions in the outermost layer of the (001) surface. This makes effective binding with the electrolyte molecule difficult. Although our computational methods and resources limit us from simulating the interface reactions over extended periods, the initial stages of these reactions have been effectively captured. This early insight is crucial for further elucidating the mechanisms of interface reactions and for enhancing the properties of cathode materials. Furthermore, given that cathode materials are subjected to frequent charge and discharge cycles, the study of the interface reactions of Li_2MnO_3 cathode materials during the charging process will be a focal point of our future research.

Data availability

The data supporting this article have been included as part of the ESI.†

Author contributions

Xiaotong Yan: methodology, investigation, formal analysis, visualization, writing – original raft. Chunwei Zhu: methodology, writing – review & editing. Weijie Huang: methodology, writing – review & editing. Yu-Jun Zhao: conceptualization, supervision, resources, writing – review & editing, funding acquisition.

Conflicts of interest

There are no conflicts to declare.

Acknowledgements

Notes and references

1 W. He, W. Guo, H. Wu, L. Lin, Q. Liu, X. Han, Q. Xie, P. Liu, H. Zheng, L. Wang, *et al.*, *Adv. Mater.*, 2021, **33**, 2005937.

This journal is © The Royal Society of Chemistry 2024

J. Mater. Chem. A, 2024, **12**, 24401–24408 | **24407**

2 Y. Ding, Z. P. Cano, A. Yu, J. Lu and Z. Chen, *Electrochem. Energy Rev.*, 2019, **2**, 1–28.

3 W. Lee, S. Muhammad, C. Sergey, H. Lee, J. Yoon, Y.-M. Kang and W.-S. Yoon, *Angew. Chem., Int. Ed.*, 2020, **59**, 2578–2605.

4 N. Guerrini, L. Jin, J. G. Lozano, K. Luo, A. Sobkowiak, K. Tsuruta, F. Massel, L.-C. Duda, M. R. Roberts and P. G. Bruce, *Chem. Mater.*, 2020, **32**, 3733–3740.

5 J. Song, H. Wang, Y. Zuo, K. Zhang, T. Yang, Y. Yang, C. Gao, T. Chen, G. Feng, Z. Jiang, *et al.*, *Electrochem. Energy Rev.*, 2023, **6**, 20.

6 Y. Lei, J. Ni, Z. Hu, Z. Wang, F. Gui, B. Li, P. Ming, C. Zhang, Y. Elias, D. Aurbach, *et al.*, *Adv. Energy Mater.*, 2020, **10**, 2002506.

7 S. Sharifi-Asl, J. Lu, K. Amine and R. Shahbazian-Yassar, *Adv. Energy Mater.*, 2019, **9**, 1900551.

8 E. Cho, K. Kim, C. Jung, S.-W. Seo, K. Min, H. S. Lee, G.-S. Park and J. Shin, *J. Phys. Chem. C*, 2017, **121**, 21118–21127.

9 P. Yan, L. Xiao, J. Zheng, Y. Zhou, Y. He, X. Zu, S. X. Mao, J. Xiao, F. Gao, J.-G. Zhang, *et al.*, *Chem. Mater.*, 2015, **27**, 975–982.

10 Y. Li, Z. Shi, B. Qiu, J. Zhao, X. Li, Y. Zhang, T. Li, Q. Gu, J. Gao and Z. Liu, *Adv. Funct. Mater.*, 2023, **33**, 2302236.

11 H.-X. Wei, Y.-M. Liu, Y.-H. Luo, Y.-D. Huang, L.-B. Tang, Z.-Y. Wang, C. Yan, J. Mao, K.-H. Dai, Q. Wu, *et al.*, *Adv. Funct. Mater.*, 2024, **34**, 2307583.

12 Q. Chen, Y. Pei, H. Chen, Y. Song, L. Zhen, C.-Y. Xu, P. Xiao and G. Henkelman, *Nat. Commun.*, 2020, **11**, 3411.

13 M. Si, D. Wang, R. Zhao, D. Pan, C. Zhang, C. Yu, X. Lu, H. Zhao and Y. Bai, *Advanced Science*, 2020, **7**, 1902538.

14 Z. Zhu, D. Yu, Y. Yang, C. Su, Y. Huang, Y. Dong, I. Waluyo, B. Wang, A. Hunt, X. Yao, *et al.*, *Nat. Energy*, 2019, **4**, 1049–1058.

15 Z. Ye, B. Zhang, T. Chen, Z. Wu, D. Wang, W. Xiang, Y. Sun, Y. Liu, Y. Liu, J. Zhang, *et al.*, *Angew. Chem., Int. Ed.*, 2021, **60**, 23248–23255.

16 Y. Shin, W. H. Kan, M. Aykol, J. K. Papp, B. D. McCloskey, G. Chen and K. A. Persson, *Nat. Commun.*, 2018, **9**, 4597.

17 P. Yan, J. Zheng, X. Zhang, R. Xu, K. Amine, J. Xiao, J.-G. Zhang and C.-M. Wang, *Chem. Mater.*, 2016, **28**, 857–863.

18 S. Zhao, B. Sun, K. Yan, J. Zhang, C. Wang and G. Wang, *ACS Appl. Mater. Interfaces*, 2018, **10**, 33260–33268.

19 S. Jeong, K. Choi, V.-C. Ho, J. Cho, J.-S. Bae, S. C. Nam, T. Yim and J. Mun, *Chem. Eng. J.*, 2022, **434**, 134577.

20 J. Liu, Z. Wu, M. Yu, H. Hu, Y. Zhang, K. Zhang, Z. Du, F. Cheng and J. Chen, *Small*, 2022, **18**, 2106337.

21 W. He, P. Liu, B. Qu, Z. Zheng, H. Zheng, P. Deng, P. Li, S. Li, H. Huang, L. Wang, *et al.*, *Advanced Science*, 2019, **6**, 1802114.

22 W. Guo, Y. Zhang, L. Lin, Y. Liu, M. Fan, G. Gao, S. Wang, B. Sa, J. Lin, Q. Luo, *et al.*, *Small*, 2023, **19**, 2300175.

23 D. Luo, H. Xie, F. Tan, X. Ding, J. Cui, X. Xie, C. Liu and Z. Lin, *Angew. Chem., Int. Ed.*, 2022, **61**, e202203698.

24 Y. Yan, S. Zhou, Y. Zheng, H. Zhang, J. Chen, G. Zeng, B. Zhang, Y. Tang, Q. Zheng, C. Wang, *et al.*, *Adv. Funct. Mater.*, 2024, **34**, 2310799.

25 J. F. Browning, L. Baggetto, K. L. Jungjohann, Y. Wang, W. E. Tenhaeff, J. K. Keum, D. L. Wood III and G. M. Veith, *ACS Appl. Mater. Interfaces*, 2014, **6**, 18569–18576.

26 W. Lu, J. Zhang, J. Xu, X. Wu and L. Chen, *ACS Appl. Mater. Interfaces*, 2017, **9**, 19313–19318.

27 K. T. Butler, G. Sai Gautam and P. Canepa, *npj Comput. Mater.*, 2019, **5**, 19.

28 S. Shi, J. Gao, Y. Liu, Y. Zhao, Q. Wu, W. Ju, C. Ouyang and R. Xiao, *Chin. Phys. B*, 2015, **25**, 018212.

29 K. Leung, *J. Phys. Chem. C*, 2012, **116**, 9852–9861.

30 T. Tamura, M. Kohyama and S. Ogata, *Phys. Rev. B*, 2017, **96**, 035107.

31 J. L. Tebbe, T. F. Fuerst and C. B. Musgrave, *ACS Appl. Mater. Interfaces*, 2016, **8**, 26664–26674.

32 B. Zhang, Z. Lin, H. Chen, L.-W. Wang and F. Pan, *J. Mater. Chem. A*, 2020, **8**, 2613–2617.

33 X. Qin, P. B. Balbuena and M. Shao, *J. Phys. Chem. C*, 2019, **123**, 14449–14458.

34 K.-Y. Lin, S. Nachimuthu, H.-W. Huang and J.-C. Jiang, *npj Comput. Mater.*, 2022, **8**, 210.

35 X. Yan, X. Zhou, C. Zhu, W. Huang and Y.-J. Zhao, *J. Mater. Chem. A*, 2024, **12**, 3722–3733.

36 G. Kresse and D. Joubert, *Phys. Rev. B: Condens. Matter Mater. Phys.*, 1999, **59**, 1758.

37 G. Kresse and J. Furthmüller, *Comput. Mater. Sci.*, 1996, **6**, 15–50.

38 G. Kresse and J. Furthmüller, *Phys. Rev. B: Condens. Matter Mater. Phys.*, 1996, **54**, 11169.

39 J. P. Perdew, K. Burke and M. Ernzerhof, *Phys. Rev. Lett.*, 1996, **77**, 3865.

40 E. P. Kamphaus, S. Angarita-Gomez, X. Qin, M. Shao, M. Engelhard, K. T. Mueller, V. Murugesan and P. B. Balbuena, *ACS Appl. Mater. Interfaces*, 2019, **11**, 31467–31476.

41 S.-H. Pan, K.-Y. Lin, W.-X. Wu, B. J. Hwang and J.-C. Jiang, *ACS Appl. Energy Mater.*, 2023, **6**, 3291–3300.

42 S. Angarita-Gomez and P. B. Balbuena, *ACS Appl. Mater. Interfaces*, 2022, **14**, 56758–56766.

43 D. Kuai and P. B. Balbuena, *ACS Appl. Mater. Interfaces*, 2022, **14**, 2817–2824.

44 J. Si and Y. Ma, *J. Phys. Chem. C*, 2023, **127**, 23541–23550.

45 S. Grimme, S. Ehrlich and L. Goerigk, *J. Comput. Chem.*, 2011, **32**, 1456–1465.

46 G. Henkelman, B. P. Uberuaga and H. Jónsson, *J. Chem. Phys.*, 2000, **113**, 9901–9904.

47 V. I. Anisimov, J. Zaanen and O. K. Andersen, *Phys. Rev. B: Condens. Matter Mater. Phys.*, 1991, **44**, 943.

48 F. Zhou, M. Cococcioni, C. A. Marianetti, D. Morgan and G. Ceder, *Phys. Rev. B: Condens. Matter Mater. Phys.*, 2004, **70**, 235121.

49 M. Ranjeh, M. Masjedi-Arani, M. Salavati-Niasari and H. Moayedi, *J. Mol. Liq.*, 2020, **300**, 112292.

50 A. Quesne-Turin, D. Flahaut, G. S. Vallverdu, L. Croguennec, J. Allouche, F. Weill, M. Ménétrier and I. Baraille, *Appl. Surf. Sci.*, 2021, **542**, 148514.

24408 | *J. Mater. Chem. A*, 2024, **12**, 24401–24408

This journal is © The Royal Society of Chemistry 2024